Contents lists available at ScienceDirect

Surfaces and Interfaces

journal homepage: www.elsevier.com/locate/surfin

Evolution of the chemical composition of Sn thin films heated during x-ray photoelectron spectroscopy

Fortunate Modiba[a,b], Christopher J. Arendse[b,*], Clive J. Oliphant[a,b,*], Werner A. Jordaan[a], Louise Mostert[a]

[a] Materials Characterization, National Metrology Institute of South Africa, Private Bag X34, Lynwood Ridge, Pretoria 0040, South Africa
[b] Department of Physics and Astronomy, University of the Western Cape, Private Bag X17, Bellville 7535, South Africa

ARTICLE INFO

Keywords:
Depth profile
High-vacuum annealing
Nanoparticle
Agglomeration

ABSTRACT

High-vacuum XPS have been used to analyse the surface modification of a 3 nm-thick Sn thin film on Si (100) before and after annealing up to 450 °C. Increasing the XPS stage temperature led to a reduction in the amount of surface Sn and increasing amounts of O and Si. High-resolution XPS scans revealed the presence of mostly pure Sn and SnO_2 for the as-deposited Sn thin film. Increasing the XPS stage temperature to > 232 °C led to the conversion of SnO_2 to SnO and an enhancing pure Sn signal. The Si2p and SiO_2 peaks become prominent at temperatures > 350 °C, which in combination with scanning electron microscope images, signals the dewetting of the Sn film and subsequent exposure of the underlying Si (100) substrate. XPS depth profiles revealed the presence of a pure Sn metallic core encapsulated by a Sn-oxide shell. Electron microscope images shows a densely packed particulate surface features for the as-deposited Sn thin film. However, these particulate regions increase in size and are more isolated at XPS stage temperatures > 350 °C.

1. Introduction

The growing global human population and global warming concerns have necessitated the transition from fossil-fuel energy reliance to sustainable and renewable energy resources [1]. In developing countries, like South Africa, sunlight radiation of 4.5–6.5 kWh/m^2 is common in a single day and thus solar cells have been identified as major contributor towards its energy supply [2]. One-dimensional silicon nanowires (SiNWs) have been identified as an attractive candidate to improve on the performance and stability of first and second generation solar cells, while reducing the material cost that reduces the overall cost [3,4]. SiNWs have excellent anti-reflective properties, due to their broadband optical absorption by multiple scattering incidents, where its reflectance can be reduced to less than 1% in the spectral range from 400–1000 nm. An additional advantage for the use of SiNWs in solar cells is that the material quality can be relaxed since the required transport length of the minority carriers are also reduced. SiNWs have also shown great promise as the anode material in high capacity Li-ion batteries [5,6].

Chemical vapour deposition (CVD), which relies on the vapour-liquid-solid (VLS) mechanism, is the most common bottom-up approach [7,8] for the deposition of SiNWs with atomic precision, which is impossible to produce with top-down methods. Briefly, the VLS mechanism proceeds sequentially from the adsorption of gaseous Si species onto the surface of a molten metal nanoparticle catalyst, to the diffusion of Si through the catalyst to the eventual nucleation and extrusion of Si in the form of a nanowire. Hence, the nanoparticle metal catalyst plays a key role during the synthesis of the SiNW as it allows for control over the nanowire diameter, chemical properties and the optoelectronic properties of the SiNWs [9].

The ideal SiNW diameter is expected be < 10 nm to effectively trap light in solar cell applications [10]. According to Wagner and Ellis [8], the formation of the Au catalyst nanoparticles occurred during heating of a Au coated Si substrate above its eutectic temperature of ~ 363 °C. The formation of the nanoparticles is a thermodynamic process, implying that it becomes difficult to manipulate the nanoparticle size during their formation. The increase in the heating temperature can lead to Ostwald ripening wherein the small particles agglomerate to form bigger particles due to strong van der Wall attractive forces between the nanoparticles. The larger particles are formed as they are energetically favourable, which ultimately results in broader Si wires [10]. The size of the nanoparticles can be influenced by using high temperatures, which can lead to smaller particle diameters, depending on the thickness of the film.

* Corresponding authors at: Department of Physics and Astronomy, University of the Western Cape, Private Bag X17, Bellville 7535, South Africa.
E-mail addresses: cjarendse@uwc.ac.za (C.J. Arendse), coliphant@nmisa.org (C.J. Oliphant).

https://doi.org/10.1016/j.surfin.2019.100378
Received 9 May 2019; Received in revised form 29 August 2019; Accepted 30 August 2019
Available online 30 August 2019

In combination with the substrate temperature, the catalyst film thickness also affects the size of the metallic catalyst nanoparticles. Al-Taay et al. [11] reported that the annealing of a thermally evaporated tin (Sn) thin film, with thicknesses of 10–100 nm, at a temperature of 400 °C can lead to the formation of metal catalyst with differing diameters. Specifically, metal nanoparticles sized 60–110 nm, 80–130 nm and 160–220 nm corresponded to film thicknesses of 10 nm, 20 nm and 100 nm, respectively.

In this study we will be investigate Sn as a candidate for catalysing SiNWs over the generally used Au catalyst. In contrast to Au, Sn has a low Sn-Si alloy eutectic temperature of about 232 °C, which is useful for microelectronic device fabrication at low substrate temperatures and power consumption [12,13]. In addition, the Sn catalyst does not form a deep level impurity in SiNWs and is more affordable as compared to Au.

Advanced analytical techniques such as x-ray photoelectron spectroscopy (XPS) and scanning electron microscopy (SEM) are used [11] to investigate and control the morphology, size and dimensions of the metal catalyst at nanoscale [11,14,15,16,17]. Despite the promising result of achieving reduced SiNW diameters with a decreasing metal film thickness, there is a lack of studies focusing on annealing Sn thin films with thickness below 5 nm. Furthermore, modern XPS systems allow for surface analysis of materials while being heated by the XPS sample stage. This study is therefore focuses on the XPS chemical analysis of a 3 nm-thick Sn thin film annealed at different temperatures during the XPS measurements and the subsequent chemical depth profiling thereof.

2. Materials and methods

A Sn thin film of thickness ~ 3 nm was thermally evaporated on single-sided polished silicon <100> wafer using an ultra-high vacuum thermal evaporator, with a base pressure of 10^{-7} mbar and a deposition rate ~ 1 Å/s. Prior to the deposition, the Si wafer was cleaned with ultrasonic agitation for 5 min sequentially in a bath containing acetone then ethanol and then deionized water. Afterwards, the Si wafers were dipped in a 5% Hydrofluoric acid for 1 min then allowed to air dry.

The Sn coated Si wafers were then annealed under XPS vacuum at typical pressures of < 10^{-8} mbar. XPS analysis was conducted in a Thermo Scientific ESCALAB 250Xi with a monochromatic Al K_α (1487 eV) x-ray beam. The calibration or peak shift analysis was done using the valence band spectra instead of the carbon peak shift since carbon was monitored as part of the analysis. In comparing the carbon and the valence peak shift, no inconsistency was observed. The annealing temperatures amounting to 180, 232, 350 and 450 °C for the XPS analysis were selected based on typical CVD synthesis conditions and the Sn-Si phase diagram. The annealed Sn thin film samples were profiled to determine the depth distribution of atomic species. A low energy (2 kV) monatomic Ar^+ beam was used to reduce as much ion beam damage as possible and preserve chemical information of the Sn thin film. The sputtering analysis was conducted using an x-ray spot size of 900 μm. Scanning electron microscopy (SEM) was used afterwards to investigate the surface morphology of the annealed Sn films. The SEM analysis was conducted using a Zeiss Crossbeam 540 and Zeiss LEO 1525 FEGSEM. Windowless EDS was used for elemental identification on the surface, which can detect at a surface of < 2 nm at a low acceleration voltage of 1.5 keV.

3. Results and discussion

Fig. 1 illustrates an overview of the chemical bonds detected on the film surface during XPS wide scans at different XPS sample holder temperatures. The spectra contain two basic types of peaks corresponding to the photoemission from the core and valence levels of Sn and Si electrons. The Sn3d peak has $Sn3d^{5/2}$ and $Sn3d^{3/2}$ doublets that is separated by a binding energy of approximately 8.5 eV. The $Sn3d^{5/2}$ and $Sn3d^{3/2}$ peaks are accompanied by O1s and C1s peaks, indicating surface oxidation and contaminations of the thin film. The carbon peak (adventitious carbon) is the result of contamination during the transfer the sample. The $Sn3d^{5/2}$ peaks reduce in intensity as the temperature increases, accompanied by an increase in the Si2p peak. This trend can be attributed to the growth in the Sn nanoparticle size through Ostwald ripening, thereby exposing more of the Si substrate. The quantitative analysis was done using the low pass energy, which indicates the high-resolution (HR) of each peak of interest. The HR spectra will reveal the chemical composition/or bond of each element detected in the survey results.

Fig. 2 displays an overlaid HR spectra of Sn and O in the as-deposited state and after annealing at 180, 232, 350, and 450 °C. The HR spectra were deconvoluted using a Gaussian–Lorentzian profile shape. The HR deconvoluted Sn peaks were centred at 485.3 eV and 486.7 eV, which correspond to pure Sn and SnO_2, respectively. At temperatures ≤ 232 °C the SnO_2 bond has a stable intensity, which is indicative of oxidation during the transfer of the sample from the thermal evaporator to the XPS system. As the temperature increases to 350 °C, the SnO_2 is reduced to SnO while the pure Sn peak increases in its intensity. This is attributed to the Sn oxides that are removed by the temperature increase, thereby exposing the pure underlying Sn. At 450 °C it was observed that the pure Sn oxidises to SnO, which is due to its exposure to the oxide that resides at the Sn-Si interface.

From the oxygen HR spectra, surface oxidation is observed as there is a metal oxide peak at room temperature. The metal oxide can be assigned to the oxidised Sn thin film as it was also observed in the Sn spectra. At 180 °C, a peak is formed with the binding energy of 532.8 eV, which corresponds with SiO_2, O-(C-H) bond/compound. At a temperature of 350 °C, the SiO_2 peak becomes broader and more intense as compared to the metal oxide peak, which can be the O at the Si/Sn interface. The SiO_2 originate from the Si substrate. At 450 °C only the SiO_2 peak at 534.2 eV was detected, which corresponds to the exposure of the Si substrate due to the agglomeration and separation of the Sn nanoparticles. According to Floro et al. [18], the presence of the SiO_2 peak can also indicate the Volmer–Weber thin film growth. Even though the Si wafer was dipped into hydrofluoric acid (HF) to remove the oxide, the Si can be easily oxidised due to atmospheric air exposure if it is not completely covered with the thin film, as is expected for a ~ 3 nm Sn thin film on a Si substrate. The XPS results reveal major chemical changes of the Sn thin film at annealing temperatures of 350 and 450 °C. According to the XPS survey results, the sample model contains the elements in order of O, Sn, O, Si, which is demonstrated in Fig. 3.

Fig. 4 shows the fitted HR spectra of the as-deposited Sn film that containes O and Si. T At temperatures < 232 °C, the SnO_2 become a stable oxidation state of Sn, indicative of oxidation during the transfer of the sample from the thermal evaporator to the XPS system. The O1s spectra reveal the metal oxide, which is consistent with the SnO/SnO_2 with a binding energy of 531.3 eV and more intense than the SiO_2 peak that originate from the Si substarte at binding energy of 532.5 eV. The Si2p spectrum indicates the pure Si2p deconvoluted into $Si2p^{1/2}$ and $Si2p^{3/2}$ double spin-orbital, which are separated by 0.6 eV with the intensity ratio of 0.5. The asymmetric Si peak is observed at the temperatures < 232 °C. A low-intensity Si-oxide peak is also present in the as-deposuted film at a binding energy of 102.2 eV.

Fig. 5 shows the fitted HR spectra at 350 and 450 °C for Sn, O and Si. As the temperature increases from 350 to 450 °C, the SnO_2 in the $Sn3d^{5/2}$ configuration was converted to SnO, while the intensity of the pure Sn peak increases. This is attributed to the Sn-oxides removed by the high temperature that in turn exposes the pure underlying Sn. At 450 °C, the pure Sn oxidises to SnO, which can be due to the exposure of O residing at the Sn and Si interface as alluded to in Fig. 6. The O1s spectra at 350 °C shows a broad SiO_2 peak with low intensity as compared to the metal oxide peak. At 450 °C, the metal oxide is no longer visible and only the SiO_2 remains, which is due to the Si substrate exposure that indicate a Sn nanoparticle growth/agglomeration or the removal of the

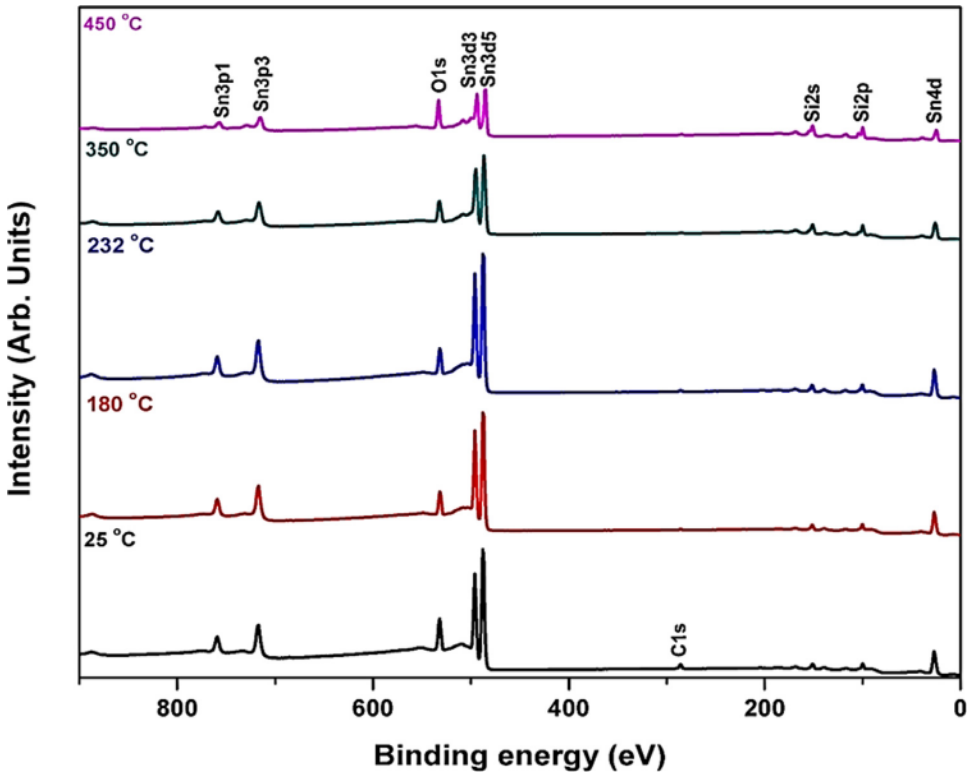

Fig. 1. XPS survey spectra of the as-deposited thin film and after annealing at 180, 232, 350, and 450 °C.

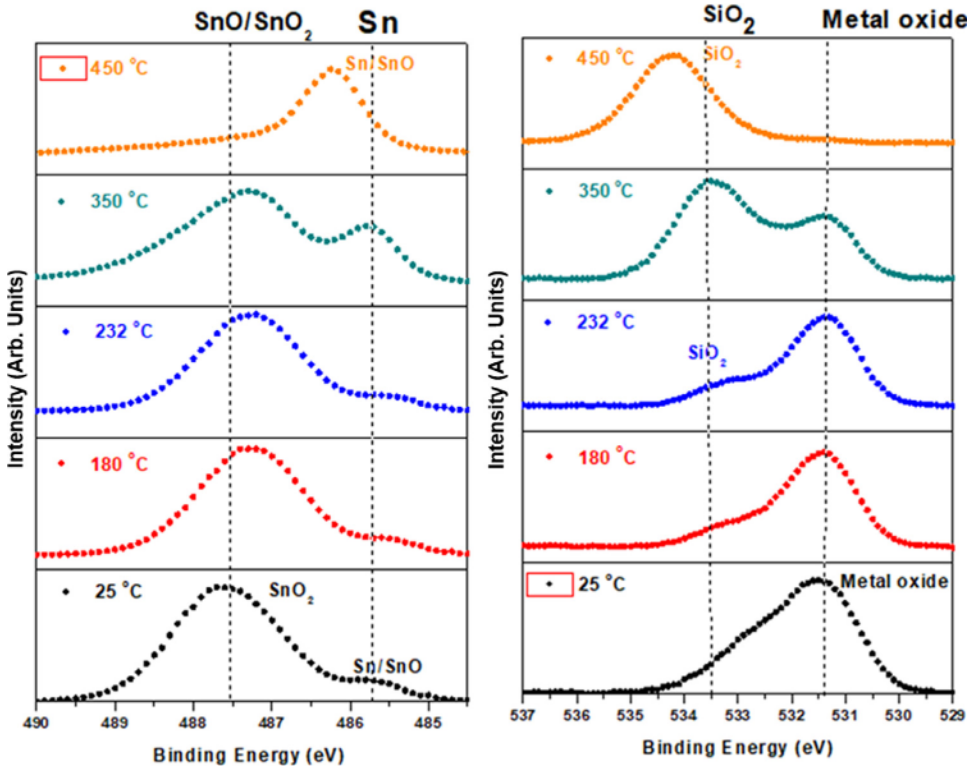

Fig. 2. High-resolution XPS spectra of (a) Sn and (b) O in the as-deposited thin film and after annealing at 180, 232, 350, and 450 °C.

Sn-oxides. The Si2p spectra at 350 °C displays an increase in intensity of the SiO_2 peak, indicative of the substrate surface oxides. The SiO_2 from the Si substrate becomes prominent at temperatures at 350–450 °C, which can be the O at the Si/Sn interface (see Fig. 3). The intense Si peaks become more defined at 450 °C, which confims the removal of O at the high temperature.

The concentration-depth profile analysis was conducted to understand the behaviour of each element with increasing temperature by sputtering the annealed sample with argon clusters in the XPS system. Fig. 6 illustrates the comparison of pure Sn and Si with their respective

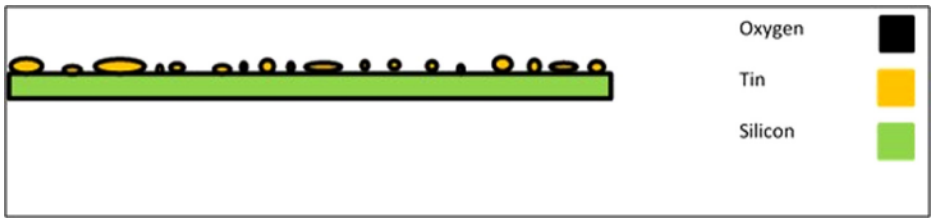

Fig. 3. Sample model.

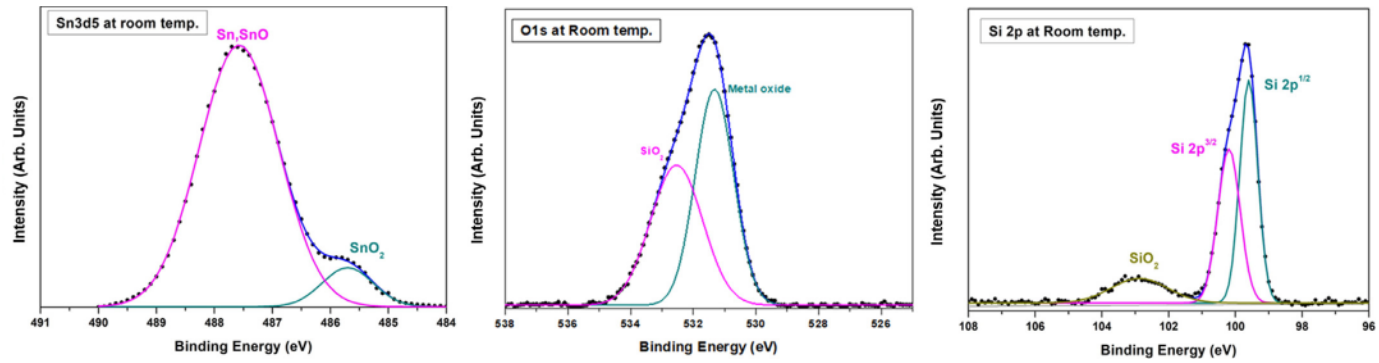

Fig. 4. High-resolution XPS spectra of Sn, O and Si bonding states of the as-deposited thin film.

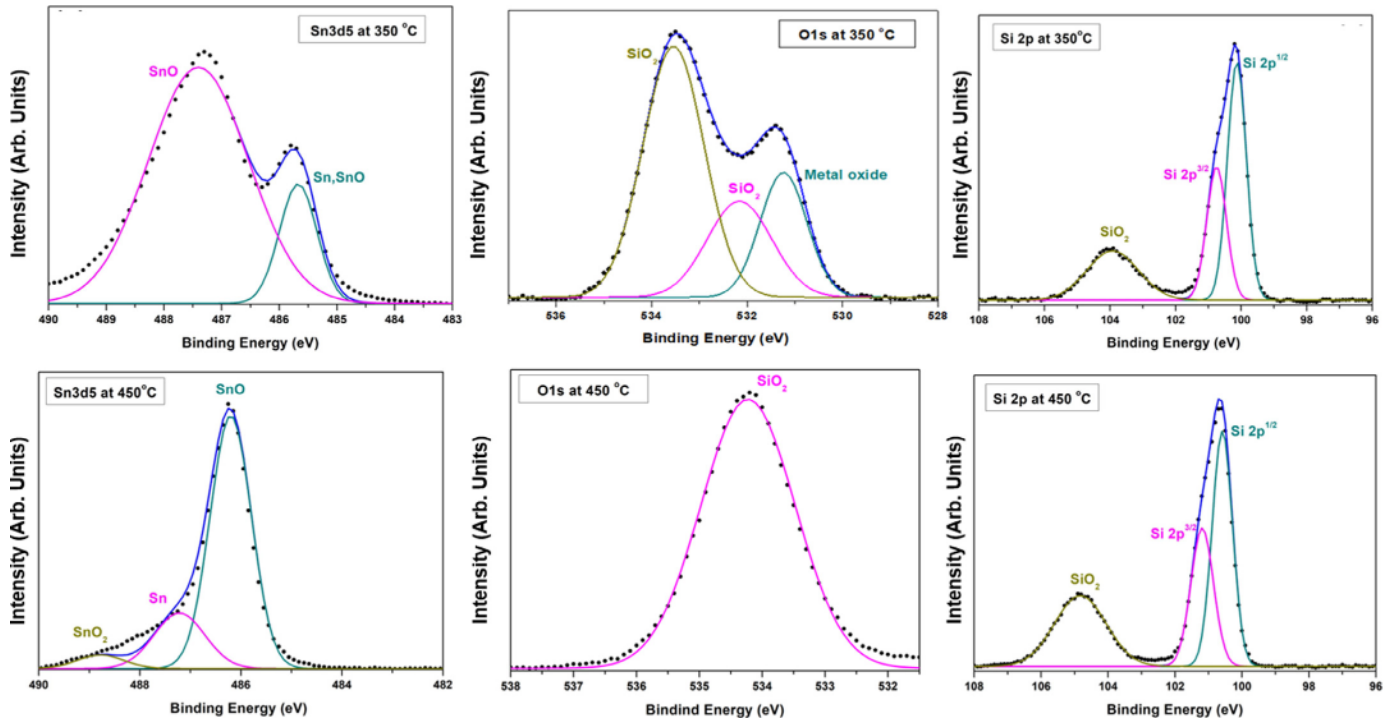

Fig. 5. High-resolution XPS spectra of Sn, O and Si bonding states after annealing at 350 and 450 °C.

oxides of the as-deposited thin film and after annealing at 350–450 °C. The oxides are the SnO_2 detected in the $Sn3d^{5/2}$, metal oxide detected in the O1s, SiO_2 detected in the Si2p and SiO_2 detected in the O1s HR spectra. The temperature increase results in the reduction in the concentration of the surface Sn and its oxides, accompanied by an increase in the concentration of the surface Si and its oxides. Moreover, the amount of pure Sn can be reduced through oxidation of which some of the O can be absorbed in the XPS vacuum system when annealed. This is observed in the decrease of the SnO_2 concentration (from the $Sn3d^{5/2}$ spectra) and its depth (sputter time is reduced from 145 s for the as-deposited to 120 s for the sample annealed at 450 °C). The SnO_2 from the $Sn3d^{5/2}$ band spectra shows no linearity in the sputter time since the 350 °C has sputtered to completion for 180 s which is longer as compared to as deposited (145 s) and 450 °C (120 s). An increase in the surface Si-concentration is evident with increasing temperature, which confirms the exposure of the Si substrate with the agglomeration and separation of the Sn nanoparticles. The SiO_2 detected in the Si2p spectra shows a marginal change with increasing temperature and extends to the Sn/Si interface.

SEM was used to investigate the evolution of the surface morphology of the Sn samples after annealing during XPS analysis. Fig. 7 shows that the as-deposited Sn film is composed of Sn nanoparticles, as confirmed by the XPS analysis. The reduction of the Sn concentration and the increase in the Si at 350 °C observed in the XPS results

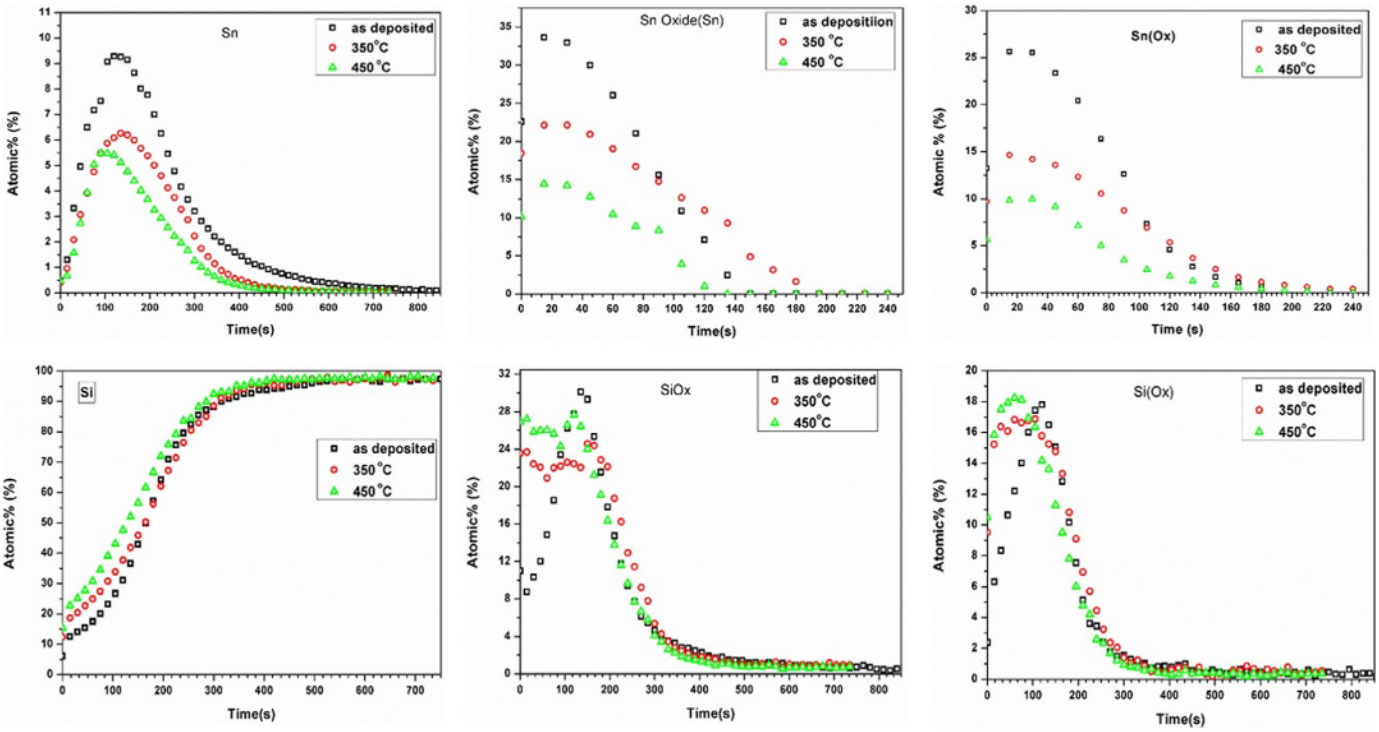

Fig. 6. XPS depth profile analysis of Sn, Si and their oxides of the as-deposited thin film and after annealing at 350 and 450 °C.

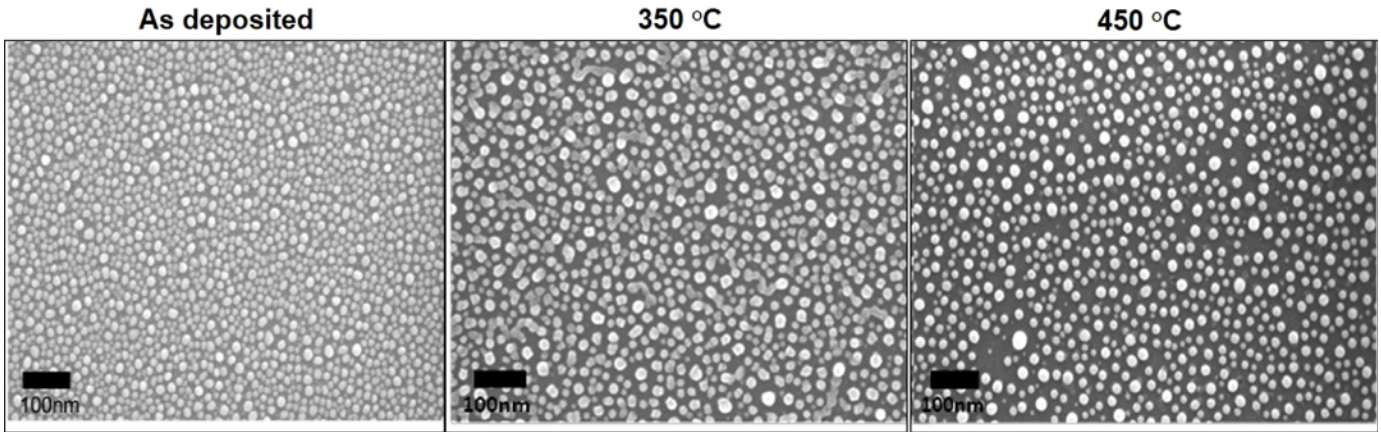

Fig. 7. SEM micrographs of the as-deposited thin film and after annealing at 350 and 450 °C.

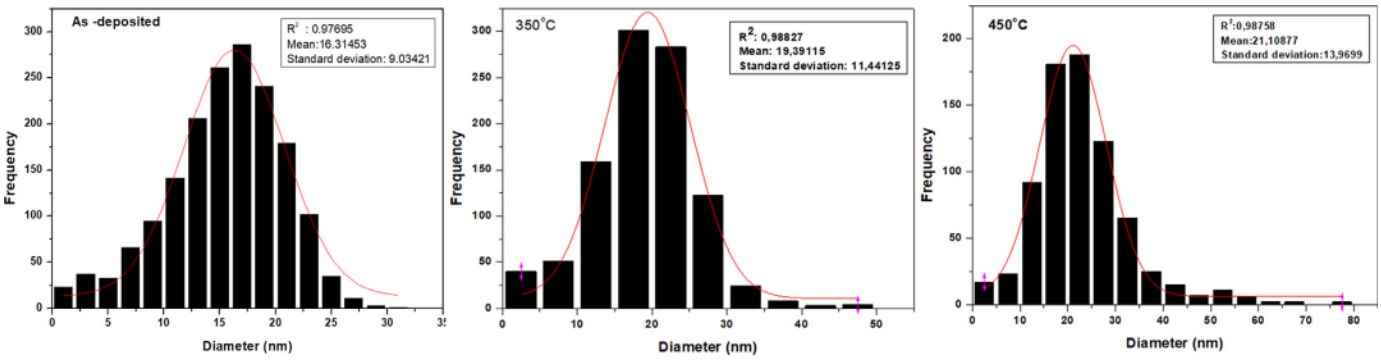

Fig. 8. Particle size distribution of the as-deposited thin film and after annealing at 350 and 450 °C.

corresponds with the formation of larger Sn nanoparticles via agglomeration which exposes the underlying Si substrate. At 450 °C the dispersion of the Sn nanoparticles and an exposed Si substrate is more pronounced. Fig. 8 shows the histogram of the particle size distribution in the as-deposited state and after annealing at 350–450 °C; and endorses the increase in the Sn nanoparticles size with increased

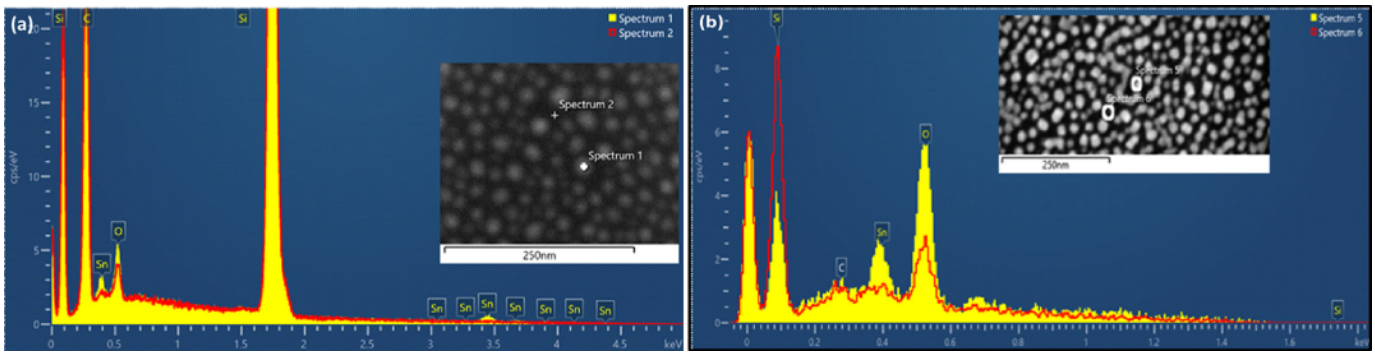

Fig. 9. Windowless EDS spectra of the (a) as-deposited thin film and (b) after annealing at 350 °C.

temperature due to surface tension, which causes strong van der Waals force between the small nanoparticles to agglomerate and form larger particles.

Fig. 9(a) shows the windowless EDS spectrum of the as-deposited sample, where spectrum 1 and 2 correspond to spot analysis performed on a Sn nanoparticle and Si substrate, respectively. Spectrum 1 confirm the Sn nanoparticle presence with an intense Si peak from the bulk Si substrate. In spectrum 2, a reduction in the Sn concentration is evident, confirming the underlying Si substrate. The surface oxidation of the Sn is inferred, as the O-peak is more intense on the Sn nanoparticle (spectrum 1) as compared to Si substrate (spectrum 2). The carbon peak is due to the contamination during the sample transfer. Fig. 9(b) displays the windowless EDS spectrum of the 350 °C sample, with similar observation for the as-deposited and 450 °C samples.

The combination of XPS and SEM analysis confirms the suitability of a 3 nm-thick Sn thin film annealed at temperatures that are generally used for the CVD of SiNWs. Particularly, the narrow size distribution and presence of a metallic Sn core occurring from room temperature to 450 °C opens the possibility of low temperature synthesis of SiNWs. The XPS depth profiling disclosed the presence of a Sn-oxide encapsulated metallic Sn core.

4. Conclusion

The chemical behaviour of Sn, O and Si elements in the sample was observed by monitoring the change in their corresponding binding energies against a varying XPS stage temperature. The as-deposited thin film consisted of metallic Sn, Si and their oxides that is attributed to the exposure to atmospheric air. The removal of adventitious carbon lead to an increased amount of Sn at 232 °C, afterwards however the formation of isolated Sn nanoparticles accompanied by an exposed Si substrate resulted in a decreased Sn surface content at and above temperatures of 350 °C. The depth profile analysis revealed the presence of Sn-oxides encapsulating a pure Sn core. This study provides valuable insight into the evolution of the Sn nano-catalyst during annealing, which will contribute towards the repeatable, low-temperature “bottom-up” chemical vapour deposition of SiNWs that can produce cheaper solar cells with improved performance.

Declaration of Competing Interest

None.

Acknowledgements

The authors acknowledge the financial support of the National Metrology Institute of South Africa and the National Research Foundation (GUN: 93212, 92520, 103621).

References

[1] P.A. O'Connor, Energy Transitions, Boston University, Boston, 2010.
[2] O.M. Popoola, C. Burnier, Solar water heater contribution to energy savings in higher education institutions: impact analysis, J. Energy South. Afr. 25 (1) (2014) 51–58.
[3] M.K. Sahoo, P. Kale, Integration of silicon nanowires in solar cell structure for efficiency enhancement: a review, J. Mater. 5 (2019) 34–48 https://doi.org/10.1016/j.jmat.2018.11.007.
[4] M. Šilhavík, M. Müller, J. Stuchlík, H. Stuchlíková, M. Klementová, J. Kočka, A. Fejfar, J. Cervenka, Comparative study of catalyst-induced doping and metal incorporation in silicon nanowires, Appl. Phys. Lett. 114 (2019) 132103https://doi.org/10.1063/1.5086617.
[5] F. Wanga, Y. Dengb, C. Yuana, Life cycle environmental impact of high-capacity lithium ion battery with silicon nanowires anode for electric vehicles, Environ. Sci. Technol. 48 (2014) 3047–3055 https://doi.org/10.1021/es4037786.
[6] A.M. Chockla, K.C. Klavetter, C.B. Mullins, B.A. Korgel, Tin-Seeded silicon nanowires for high capacity li-ion batteries, Chem. Mater. 24 (2012) 3738–3745 https://doi.org/10.1021/cm301968b.
[7] P.R. Bandaru, P. Pichanusakorn, An outline of the synthesis and properties of silicon nanowires, Semicond. Sci. Technol. 25 (2010) 024003https://doi.org/10.1088/0268-1242/25/2/024003.
[8] R.S. Wagner, W.C. Ellis, "Vapour-liquid-solid mechanism of single crystal growth, Appl. Phys. Lett. 4 (1964) 89–90.
[9] H.J. Choi, Vapor–liquid–solid growth of semiconductor nanowires, in: G.C. Yi (Ed.), Semiconductor Nanostructures for Optoelectronic Devices, Springer, Berlin, 2012, pp. 1–36.
[10] W.S. Shi, Y.F. Zheng, N. Wang, C.S. Lee, S.T. Lee, A general synthetic route to III–V compound semiconductor nanowires, Adv. Mater. 13 (2001) 591–594 https://doi.org/10.1002/chin.200130239.
[11] H.F. Al-Taay, M.A. Mahdi, D. Parlevliet, P. Jennings, Controlling the diameter of silicon nanowires grown using a tin catalyst, Mater. Sci. Semicond. Process. 16 (2013) 15–22 https://doi.org/10.1016/j.mssp.2012.07.006.
[12] F. Lacopi, P.M. Vereecken, M. Schaekers, M. Caymax, N. Moelans, B. Blanpain, O. Richard, C. Detavernier, H. Griffiths, Plasma-enhanced chemical vapour deposition growth of Si nanowires with low melting point metal catalysts: an effective alternative to Au-mediated growth, Nanotechnology 18 (2007) 505307https://doi.org/10.1088/0957-4484/18/50/505307.
[13] M. Jeon, H. Uchiyama, K. Kainisako, Characterization of Tin-catalyzed silicon nanowires synthesized by the hydrogen radical-assisted deposition method, Mater. Lett. 63 (2009) 246–248 https://doi.org/10.1016/j.matlet.2008.10.005.
[14] Y.G. Jung, S. Jee, J.H. Lee, Effect of oxide thickness on the low temperature (≤ 400°C) growth of cone-shaped silicon nanowires, J. Appl. Phys. 102 (2007) 046102–046102-3 https://doi.org/10.1063/1.2769267.
[15] J. Abad, C. Gonzalez, P.L. de Andres, E. Roman, Characterization of thin silicon overlayers on rutile tio_2 (110) − (1 × 1), Phys. Rev. B 82 (2010) 165420https://doi.org/10.1103/PhysRevB.82.165420.
[16] M. Kwoka, M. Krzywiecki, Impact of air exposure and annealing on the chemical and electronic properties of the surface of SnO_2 nanolayers deposited by rheotaxial growth and vacuum oxidation, Beilstein J. Nanotech. 8 (2017) 514–521 https://doi.org/10.3762/bjnano.8.55.
[17] A. Thøgersen, J.H. Selj, E.S. Marstein, Oxidation effects on graded porous silicon anti-reflection coatings, J. Electrochem. Soc. 159 (2012) D276–D281 https://doi.org/10.1149/2.jes113659.
[18] J.A. Floro, E. Chason, R.C. Cammarata, D.J. Srolovitz, Physical origins of intrinsic stresses in Volmer-Weber thin films, MRS Bull. 27 (2002) 19–25 https://doi.org/10.1557/mrs2002.15.